J Membrane Biol (2015) 248:517–527
DOI 10.1007/s00232-015-9798-5

Decreasing Transmembrane Segment Length Greatly Decreases Perfringolysin O Pore Size

Qingqing Lin[1] · Tong Wang[2] · Huilin Li[1,2] · Erwin London[1]

Received: 6 January 2015 / Accepted: 25 March 2015 / Published online: 8 April 2015

Abstract Perfringolysin O (PFO) is a transmembrane (TM) β-barrel protein that inserts into mammalian cell membranes. Once inserted into membranes, PFO assembles into pore-forming oligomers containing 30–50 PFO monomers. These form a pore of up to 300 Å, far exceeding the size of most other proteinaceous pores. In this study, we found that altering PFO TM segment length can alter the size of PFO pores. A PFO mutant with lengthened TM segments oligomerized to a similar extent as wild-type PFO, and exhibited pore-forming activity and a pore size very similar to wild-type PFO as measured by electron microscopy and a leakage assay. In contrast, PFO with shortened TM segments exhibited a large reduction in pore-forming activity and pore size. This suggests that the interaction between TM segments can greatly affect the size of pores formed by TM β-barrel proteins. PFO may be a promising candidate for engineering pore size for various applications.

Keywords Cholesterol-dependent cytolysin · Bacterial toxin proteins · Cholesterol · Transmembrane protein · Hydrophobic mismatch

Electronic supplementary material The online version of this article (doi:10.1007/s00232-015-9798-5) contains supplementary material, which is available to authorized users.

✉ Erwin London
erwin.london@stonybrook.edu

[1] Department of Biochemistry and Cell Biology, Stony Brook University, Stony Brook, NY 11794-5215, USA

[2] Biosciences Department, Brookhaven National Laboratory, Upton, NY 11973, USA

Introduction

Perfringolysin O (PFO) belongs to the family of cholesterol-dependent cytolysins (CDCs). CDCs contribute to the pathogenesis of a large number of Gram-positive bacterial pathogens (Parker and Feil 2005; Aroian and Van Der Goot 2007). These toxins bind to cholesterol in the membranes of eukaryotic cells and oligomerize into ring-shaped structures, estimated to contain 30–50 subunits, which surround pores of ~30–35-nm diameter (Tweten 2005; Hotze and Tweten 2012). This size by far exceeds that of most other large proteinaceous pores, e.g., staphylococcal α-toxin with a central pit of 2–3 nm in diameter (Fussle et al. 1981), or even the complement membrane attack complex with an internal pore up to 10 nm (Bhakdi and Tranum-Jensen 1984). PFO pores permit flux of both ions and macromolecules, and the toxin has become a popular tool for the controlled permeabilization of cell membranes (Cassidy and O'riordan 2013).

Crystallographic studies on PFO show that the monomeric toxin molecule is elongated and contains four domains (named domains 1–4) rich in β-sheet structure (Rossjohn et al. 1997). Upon binding to a target membrane, bound PFO molecules diffuse laterally and interact with each other to form a prepore complex (Shepard et al. 2000). Subsequently, a profound conformational change occurs that results in the formation of the transmembrane (TM) pore. Using a combination of cysteine scanning and fluorescence spectroscopy, Shepard et al. (1998) and Shatursky et al. (1999) identified the membrane-spanning region of PFO. Two sets of α-helical bundles that flank the domain 3 core β-sheets, which extend from the domain 3 core β-strands 1–4, undergo a change in their secondary structure to form two amphipathic β-hairpins. Shatursky et al. (1999) further showed that these twin hairpins spanned

the bilayer. Each TM hairpin (which has been designed by the term TMH Shatursky et al. 1999) is approximately 30 residues long, and contains two β-strands. In a previous study, we showed that altering the length of PFO TM segments affects PFO localization into liquid-ordered or liquid-disordered membrane microdomains (Lin and London 2013). PFO mutants with lengthened or shortened TM segments also exhibited different pore formation activity, which was dependent on membrane thickness. Here, we report that altering the length of PFO TM segments can unexpectedly alter pore and oligomer size. This is of interest because it has implications for bioengineering of proteins with specific pore properties. Lengthening the strand length by two residues did not greatly affect the pore or oligomer size, but did decrease the stability of oligomerization. Shortening strands by two residues had a larger effect, greatly reducing the pore and oligomer size. These findings suggest that engineering PFO TM strand length may be a promising approach to construct PFO molecules that can allow the cellular escape or delivery of macromolecules with a highly controlled size limit.

Materials and Methods

Materials

Phospholipids

1,2-dimyristoleoyl-*sn*-glycero-3-phosphocholine (DMoPC), 1,2-dioleoyl-*sn*-glycero-3-phosphocholine (DOPC), 1,2-distearoyl-*sn*-glycero-3-phosphocholine (DSPC), cholesterol (ovine wool), 1,2-[9,10-dibromo] stearoyl-*sn*-glycero-3-phosphocholine (BrPC), and 1,2-dioleoyl-*sn*-glycero-3-phosphoethanolamine-*N*-(lissamine rhodamine B sulfonyl) (Rho-DOPE) were purchased from Avanti Polar Lipids (Alabaster, AL). Lipids were stored in ethanol or chloroform at −20 °C. Concentrations were determined by dry weight or by absorbance, using an ε of 95,000 cm^{-1} M^{-1} at 560 nm for rhodamine lipids in methanol (Nelson et al. 2010). Streptavidin was purchased from GenScript (Piscataway, NJ). 4,4-difluoro-5,7-dimethyl-4-bora-3*a*,4*a*-diaza-*s*-indacene-3-propionic acid (BODIPY-FL), cascade blue (CB)-labeled dextran (CB-dextran) (molecular weight 3, 10, 70 kD) and the free cascade blue dye, 8-methoxypyrene-1,3,6-trisulfonic acid, trisodium salt (MPTS) were purchased from Molecular Probes, Invitrogen (Grand Island, NY). Biocytin (ε-biotinoyl-L-lysine) was purchased from Anaspec (San Jose, CA). All other chemicals were reagent grade. BODIPY-labeled streptavidin (BOD-SA) was prepared by following protocols developed by A. Heuck (U. Mass. Amherst). Generally, streptavidin and BODIPY-FL were mixed at 4:1 mol ratio in 0.1 M $NaHCO_3$, pH 8.3 and incubated for 2 h at room temperature. The reaction mixture was then applied to Sephadex G-50 to separate the conjugate from unreacted BODIPY-FL. The concentration of BOD-SA was determined by absorbance, using an ε of 41,326 $cm^{-1}M^{-1}$ at 280 nm.

Generation and Purification of PFO Derivatives

A functional cysteine-less derivative of wild-type PFO (PFO C459A) (Shepard et al. 1998) was a kind gift of A. Heuck, U. Mass. Amherst. PFO mutants with lengthened (long PFO) or shortened (short PFO) TM sequences were generated as previously described from the PFO C459A plasmids using site-directed ligase-independent mutagenesis (Chiu et al. 2004, 2008). Long PFO contains 2 Ala inserted at four sites between residues V202-L203, E204-N205, I298-K299, and N300-T301, and short PFO has residues K201V202, N205S206, L297I298, and T301D302 deleted (Lin and London 2013). Variants of PFO with an Ala to Cys substitution at residue 215 were generated by the QuickChange site-directed mutagenesis kit (Stratagene) as previously described (Lin and London 2013). PFO was expressed in *E. coli* BL21(DE3)pLysS and purified similarly as described previously (Nelson et al. 2008). Final purity for WT and long PFO appeared to be >95 %, and roughly ∼70–80 % for short PFO, which only expresses at low levels. The purified PFO was stored in phosphate-buffered saline (PBS, 1.8 mM KH_2PO4, 10 mM Na_2HPO4, 137 mM NaCl, and 2.7 mM KCl at pH 7.4) at a concentration of ∼1–1.5 mg/ml for WT and long PFO, or ∼0.3–0.5 mg/ml for short PFO at −20 °C.

Preparation of Lipid Vesicles

Multilamellar vesicles (MLV) were prepared with the desired mixture of lipids. Lipids in solvent were mixed, and then dried with N_2. They were then re-dissolved in $CHCl_3$ and re-dried under N_2 and then in high vacuum for at least 1 h. The re-dried lipid mixtures were dispersed in PBS, adjusted with acetic acid to pH 5.1 at 70 °C to give the desired final concentration and agitated at 55 °C for 15 min using a VWR multitube vortexer (Westchester, PA) placed within a convection oven (GCA Corp, Precision Scientific, Chicago, IL). Samples were then cooled to room temperature.

For electron microscopy (EM) measurements, large unilamellar vesicles (LUV) were prepared from MLV by subjecting the MLV to seven cycles of freezing in a mixture of dry ice and acetone and thawing at room temperature. They were then extruded through 200-nm polycarbonate filters (Avanti Polar Lipids, Alabaster, AL) 11 times to obtain LUV of relatively uniform vesicle size. LUV samples for leakage studies were prepared as described below.

Fluorescence Intensity Measurements

Fluorescence emission intensity was measured (unless otherwise noted) at room temperature on a SPEX Fluorolog 3 spectrofluorimeter. For fixed wavelength measurements, excitation and emission wavelength sets used (in nm) were (280, 340) for tryptophan; (400, 420) for CB-dextran and MPTS; (488, 515) for BODIPY-FL-labeled streptavidin (BOD-SA); and (570, 590) for Rho-DOPE. Unless otherwise noted, fluorescence intensity in single background samples lacking fluorophores was subtracted.

Assay for Biocytin Leakage

PFO-induced pore formation was measured by assaying the reaction of vesicle-trapped biocytin with externally added BOD-SA via the increase in the BODIPY fluorescence emission intensity upon binding of biocytin to BOD-SA located in the external solution, as previously described (Nelson et al. 2008). Generally, 537 μM biocytin was trapped within LUVs composed of 10 mM 6:4 (mol:mol) DOPC/cholesterol. After dialysis against 4 L PBS buffer overnight, 10 μl of vesicles was diluted with 990 μl PBS pH 5.1. Then 10 nM BOD-SA was added externally. BODIPY emission intensity was measured. Various amounts of WT, long, or short PFO were added and after a brief mixing, BODIPY intensity was monitored as a function of time for up to 40 min.

Entrapping BOD-SA, CB-Dextran, or MPTS in Model Membrane Vesicles

LUV containing trapped BOD-SA, trapped CB-dextran, or trapped MTPS was prepared similarly to as described previously (Rosconi et al. 2004; Wang and London 2009). A mixture containing 10 mM lipids comprising 45:15:40 (mol:mol:mol) DOPC/BrPC/cholesterol or 27.5:27.5:45 (mol:mol:mol) DSPC/DMoPC/cholesterol with 0.002 mol % Rho-DOPE (a fluorescent lipid marker), 70 μg/ml BOD-SA or 10 μM CD-dextran or 10 μM MPTS, and 20 mg/ml *n*-octyl-*β*-glucoside was dissolved in 1 ml PBS, pH 7.4. After removing *n*-octyl-*β*-glucoside by dialysis against 4 L PBS buffer at 4 °C overnight, the samples were extruded through 200-nm polycarbonate filters 11 times. Then a Sepharose 4B-CL column (1 cm in diameter, 25 cm in length) was used to separate free BOD-SA, CB-dextran, or MPTS from LUV-trapped BOD-SA, CB-dextran, or MPTS, respectively. After elution with PBS pH 7.4, fractions (~1 ml per fraction) containing LUV (usually fractions 6–8) were collected for experiments. Typically, the final lipid concentration was 2–4 mM as determined by Rho-DOPE fluorescence, i.e., by determining the ratio of the fluorescence of Rho-DOPE after sample preparation to that in the vesicles prior to fractionation, assuming that the loss in lipids during dialysis is minimal. Final average vesicle diameter as estimated by dynamic light scattering (Cheng and London 2011) was 130 nm.

Assay for Leakage of BOD-SA, CB-Dextran, or MPTS

The leakage of BOD-SA, CB-dextran, or MPTS was measured by diluting a 125–250 μl aliquot of LUVs containing trapped BOD-SA, CB-dextran, or MPTS to 1 ml with PBS pH 5.1 (or pH 7.4 where noted) to give a final lipid concentration ~500 μM and final pH 5.3–5.7. Then the LUVs were incubated with small aliquots containing 20 μg WT PFO, 20 μg long PFO, or 30 μg short PFO for 1 h at room temperature. Samples were then spun for 30 min in a Beckman L8-85 ultracentrifuge at 84,000×*g* at 4 °C. After centrifugation, supernatants containing leaked BOD-SA or CB-dextran or MPTS were removed, and pellets containing the LUVs were resuspended in 1 ml PBS pH 5.1. Rho-DOPE and either BOD-SA or CB fluorescence were then measured for both the supernatant and the pellet. (Calculated values have been corrected for incomplete pelleting of vesicles see below.) The efficiency of vesicle pelleting was generally about 60–70 % for vesicles without PFO, 70–80 % for short PFO, and 80–95 % for WT and long PFO.

Electron Microscopy and Image Processing

50 μg WT, long, or short PFO was incubated with 1 ml LUVs containing 500 μM lipid, composed of 6:4 (mol:mol) DOPC/cholesterol or 27.5:27.5:45 (mol:mol:mol) DSPC/DMoPC/cholesterol in PBS pH 5.1 for at least 1 h at room temperature. To prepare EM grids for negative staining, a layer of carbon film (~20 nm thick) was evaporated on a piece of freshly cleaved mica in an Edwards vacuum evaporator ($<10^{-5}$ Torr). Carbon film was then peeled off from mica by floating it on the surface of deionized water and deposited on 300 mesh copper grids. All homemade continuous carbon-coated grids were air-dried and stored for future usage. Carbon-coated grids were first glow discharged in 100 mTorr argon atmosphere for 1 min. A drop of 4 μl of sample solution was applied to the glow-discharged continuous carbon-coated EM grid and incubated for 1 min. Excess solution was removed by blotting the grid with a piece of filter paper. The grid was then washed by a drop of ddH_2O and stained in 2 % (w/v) uranyl acetate aqueous solution for 1 min. After blotting excess stain solution, the grid was air-dried. The negatively stained sample was examined in a JEOL JEM-2010F TEM

operating at 200 kV. EM images were recorded in low-dose mode (15 $e^{-}/Å^{2}$) at ×50,000 or ×60,000 microscope magnification using a Gatan UltraScan 4000 CCD camera (4096 × 4096 pixel).

Particle selection and image processing were done using EMAN and EMAN2 software package (Ludtke et al. 1999; Tang et al. 2007). Raw particle images were selected in a semi-automatic manner with *e2boxer.py* in EMAN2. The saved raw images were low-pass filtered to 2 nm and manually inspected to remove "bad" particles (low contrast, contacting other particles). Reference-free 2D classifications of image dataset were done with *refine2d.py* in EMAN.

Results

Appearance of PFO with Different Length of TM Segments in Electron Microscopy

We previously studied and characterized some of the properties of PFO with shortened and lengthened TM segments, and observed that a deletion of two residues from each of the sequences that form the TM β-strands resulted in a reduction of the extent of pore formation, while inserting two residues into them did not (Lin and London 2013). To obtain more information about the origin of this behavior, EM was used to examine whether changing the length of PFO TM segments altered the overall properties of membrane-inserted PFO. Electron micrographs of cholesterol-containing membranes showed that PFO oligomers appear as rings and partial rings called arcs (Mitsui et al. 1979; Shepard et al. 2000). When we prepared PFO under conditions giving complete cholesterol-dependent membrane insertion (Nelson et al. 2008), these structures were also seen in our samples of WT PFO. Rings had an estimated diameter of 30–40 nm, consistent with ~30–40 subunits per pore (Fig. 1a). Very similar rings and arcs were observed with long PFO (Fig. 1b). In both cases, rings and arcs were often not membrane associated, suggesting that they had fallen off from the vesicles during EM sample preparation. It should be noted that despite the similarity between the appearance of WT and long PFO oligomers, WT PFO showed the characteristic resistance to disassembly on SDS gels (Shepard et al. 2000), while long PFO oligomers dissociated into monomers on SDS gels (Supplemental Fig. 1).

In contrast to WT PFO, Fig. 1c shows that large ring-shaped or arc-shaped structures were absent from samples of short PFO mixed with lipid vesicles under conditions in which it recognizes membrane cholesterol and inserts maximally (~65 %) (Lin and London 2013). Instead, small oligomeric structures were observed. (The observation that the short PFO frequently appears to be dissociated from vesicles may reflect an even more facile tendency to dissociate from membranes relative to WT PFO due to its short TM segments, or simply low visibility of short PFO when embedded in membranes.) Given the size of these structures, and counting "blobs" of mass as a monomer, the micrographs are suggestive of the formation of tetramers (image C_2) or perhaps pentamers (image C_1) by short PFO. This is also roughly consistent with the size of these oligomers relative to the size of the larger rings formed by WT in the micrographs. These small oligomers show what appears to be a small central hole, suggesting the possibility that short PFO would form a much smaller pore than by WT or long PFO. While this is suggestive, a strong argument cannot be made based on the EM data, especially for short PFO. The short PFO oligomers are not membrane associated, which could result in them forming a structure different from that when membrane bound, and there certainly could be other potential perturbations arising from preparing samples for electron microscopy. Furthermore, we cannot rule out the possibility that the oligomers seen with short PFO simply assembled in solution. Therefore, a different approach was used to investigate PFO pores (see below).

Dose-Dependent Pore Formation by WT, Long, and Short PFO

To investigate the suggestion from EM that short PFO has different pore properties than WT and long PFO, while the pore properties of WT and long PFO are similar, we first examined the extent of pore formation by measuring the efflux of the small molecule biocytin (biotinyl-lysine) out of vesicles containing membrane-inserted PFO. Upon efflux of biocytin from vesicles, it binds to the externally added BODIPY-streptavidin (BOD-SA). This displaces the BODIPY group covalently bound to streptavidin from the biotin binding pocket on the streptavidin molecule, which results in an increase in BODIPY fluorescence (Nelson et al. 2008). As shown in Fig. 2, under conditions in which WT and long PFO have been previously shown to be fully membrane bound, and short PFO maximally membrane bound (Lin and London 2013), WT and mutant PFO formed pores in DOPC vesicles containing 40 mol% cholesterol. The extent of pore formation was protein dose dependent. This is likely to reflect an increasing fraction of vesicles containing pores as the concentration of protein is increased (see below). With increasing amounts of WT PFO added, BODIPY emission intensity plateaued at ~5 μg WT PFO with a near three-fold increase in fluorescence. Similarly, after adding 50 μl of 1:4 Triton X-100/water to the samples to dissolve the vesicles and release trapped biocytin, the BODIPY intensity increase

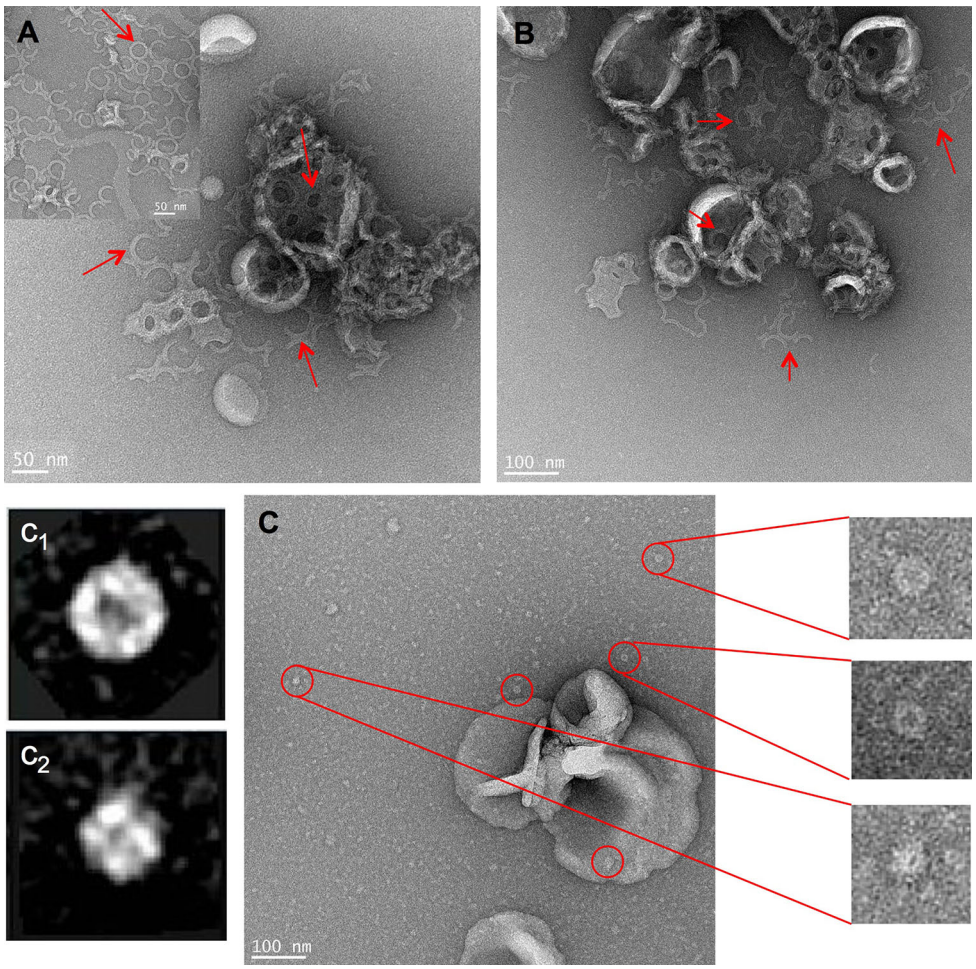

Fig. 1 EM image of PFO mutants. **a** 50 μg WT PFO in 27.5:27.5:45 (mol:mol:mol) DSPC/DMoPC/cholesterol (500 μM total lipid). *Inset* in **a** 20 μg WT PFO in 6:4 (mol:mol) DOPC/cholesterol (200 μM total lipid); **b** 50 μg long PFO in 27.5:27.5:45 (mol:mol:mol) DSPC/DMoPC/cholesterol (500 μM total lipid). **c** 50 μg short PFO in 27.5:27.5:45 (mol:mol:mol) DSPC/DMoPC/cholesterol (500 μM total lipid). Samples were prepared in PBS buffer pH 5.1. Large objects in each micrograph are lipid vesicles. *Arrows* in **a**, **b** point to full or partial PFO rings, many of which have fallen off the vesicles. *Circles* in **c** point to small oligomers, several of which are shown magnified. Averaged 2D views of those small pore particles presented in **c** are shown: (C_1) an averaged 2D view computed from 17 small pore particles; (C_2) an averaged 2D view computed from 27 small pore particles. The outer diameter of the averaged particle is ~11–15 nm. The interior lowest density region is ~2–3 nm in size

was 3- to 3.5-fold (data not shown), suggesting that the plateau reflects the point when all of the BOD-SA is bound to biocytin.

Dose-dependent pore formation by long PFO was very similar to that by WT PFO, indicating that the AlaAla insertions in each β-strand did not significantly alter the pore-forming ability, and that the WT and long PFO make pores with equal efficiency. In contrast, shortening TM segments by two residues greatly reduced pore formation by short PFO. Even after correction for the ~35 % (determined in a previous study Lin and London 2013) of short PFO that does not bind to model membranes, pore formation by short PFO was reduced about three-fold relative to WT and long PFO, i.e., three-fold to four-fold more short PFO than WT or long PFO was needed to release an equivalent amount of biocytin (Fig. 2).

PFO Derivatives with Different Length TM Segments Form Pores with Different Diameters

The difference between short PFO and WT PFO could be explained by either a decrease in pore number, pore size, or a combination of both. To investigate if pore size was altered, PFO-induced leakage of macromolecules with different sizes was measured. In the experiment shown in Fig. 3, leakage was measured using vesicles containing entrapped MPTS (MW 538), CB-dextran 3 (MW 3 kD), CB-dextran 10 (MW 10 kD), or CB-dextran 70 (MW 70 kD). The effective diameter of CB-dextran 3 in solution is estimated to be 2.8 nm, that of CB-dextran 10 to be 4.72 nm, and that of CB-dextran 70 to be 11.6 nm (Scherrer and Gerhardt 1971). LUVs containing trapped

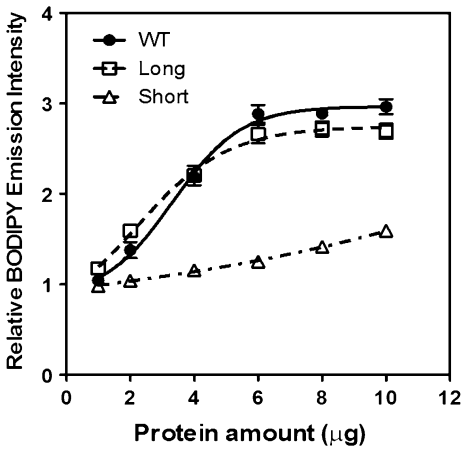

Fig. 2 Dose dependent of PFO pore formation. The *y* axis shows the increase of external BODIPY-streptavidin fluorescence after the addition of PFO relative to that before the PFO addition. Samples contained LUV composed of 6:4 mol/mol DOPC/cholesterol (100 μM total lipid) containing entrapped biocytin and 10 nM externally added BODIPY-streptavidin in PBS pH 5.1. BODIPY fluorescence was measured 40 min after the addition of PFO. Average (mean) values and, shown if larger than the size of the symbols, SD values (*error bars*) were obtained from triplicates

MPTS or dextrans were exposed to PFO. If pores are sufficiently large, efflux of entrapped molecules should result in their release into the supernatant after pelleting vesicles by centrifugation.

Using these molecules we first examined pore size in LUVs composed of DOPC/BrPC/cholesterol. (BrPC has a high density and 15 mol% BrPC was used to assist LUV pelleting this lipid mixture, which otherwise does not pellet efficiently.) The amounts of protein used were chosen to give the same amount of membrane-bound WT, short, and long PFO based on our previous studies, showing that while long and WT PFO are fully membrane bound only about 65 % of short PFO binds to membranes (Lin and London 2013), and an easily measured extent of pore formation. As shown in Fig. 3a, the pores formed by both WT and long PFO did not block the release of MPTS or CB-dextran, with almost 25 % of fluorescence from pelleted vesicles detected in the supernatant. The observation that % release is independent of dextran size indicates that partial release is not due to slow release of dextran, but rather the fact that most vesicles do not contain any pores. Confirming this, the % release of both MPTS and CB-dextran 70 by WT and long PFO was almost identical after 1 and 2 h incubation (Supplemental Fig. 2).

Pores formed by short PFO allowed the release of MPTS to a slightly lower extent than WT and long PFO. However, 3 kD dextran was released to a lower extent, and only a minimal leakage of the larger dextrans was observed. This indicates that at least some of the pores formed by short PFO are reduced in size relative to those formed by WT and long PFO. The residual leakage of large dextrans could

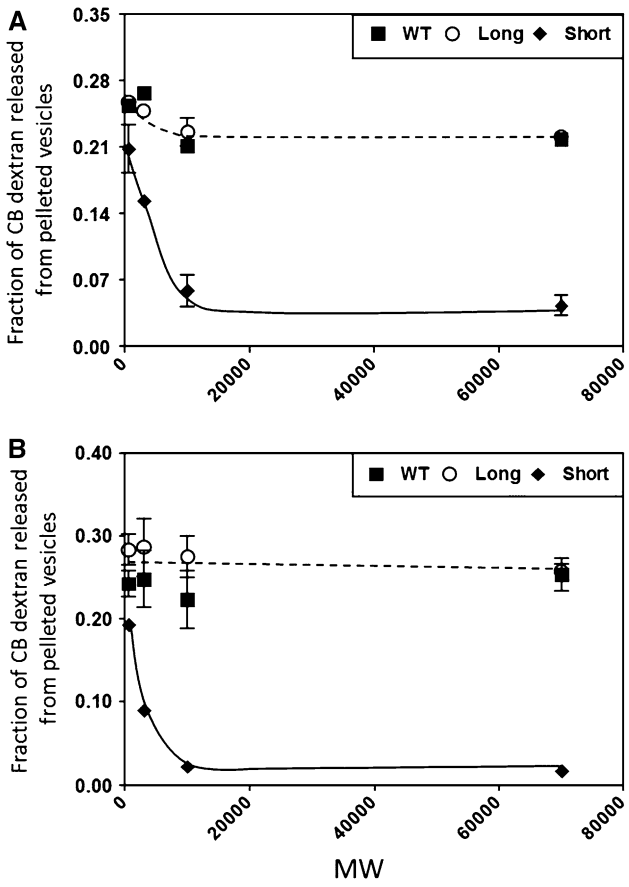

Fig. 3 Pore size of PFO mutants detected by PFO-induced CB-dextran leakage. **a** LUVs composed of 45:15:40 (mol:mol:mol) DOPC/BrPC/cholesterol with 0.002 mol% Rho-DOPE; **b** LUVs composed of 27.5:27.5:45 mol/mol/mol DSPC/DMoPC/cholesterol with 0.002 mol% Rho-DOPE. Samples containing LUVs (~500 μM lipid) having entrapped MPTS or CB-dextran without (control) or with 20 μg WT (*filled square*), 20 μg long (*open circle*), or 30 μg short (*filled diamond*) PFO were incubated for 1 h. Final pH 5.3–5.7. After centrifugation, Rho-DOPE (F_{Rho}) and MPTS/cascade blue (F_{CB}) emission intensity were measured for the resuspended pellet and supernatant. The fraction of MPTS (cascade blue dye) or CB-dextran released from those vesicles that pelleted is equal to $[F_{CB\text{-supernatant}}/(F_{CB\text{-supernatant}} + F_{CB\text{-pellet}})] - [F_{Rho\text{-supernatant}}/(F_{Rho\text{-supernatant}} + F_{Rho\text{-pellet}})]$. Pelleting was generally 60–90 % of lipid, see "Materials and Methods" section. Values shown are after subtraction of the background which is due to the amount of MPTS or CB-dextran unassociated with vesicles in the absence of PFO (the background fraction in the supernatant was ≤0.1). Average (mean) values and SD values (*error bars*) were obtained from triplicates

either mean that there is a range of pore sizes so that a few vesicles had pores large enough to allow a large dextran to escape the vesicle, or that smaller average pore size slows the release of large dextrans. The latter explanation is unlikely because the extent of leakage by 10 and 70 kD dextran was similar. Furthermore, for both MPTS and CB-dextran 70, short PFO-induced leakage was similar after 1 and 2 h incubation (Supplemental Fig. 2). Therefore, it appears that most of the pores formed by short PFO are too

small to allow molecules of 10kD or larger through, although a few larger pores form.

PFO pore size was also studied in ternary lipid mixtures (DSPC/DMoPC/cholesterol) forming a mixture of liquid-ordered (Lo) and liquid-disordered (Ld) domains. In a previous study, we demonstrated that in these lipid vesicles, WT and long PFO prefer the thick Lo domain, whereas short PFO has a higher affinity for thin Ld domain (Lin and London 2013). Vesicles with this composition were used (again under conditions giving complete binding of WT and long PFO and maximal binding of short PFO (Lin and London 2013)) to investigate whether different domain localization and/or lipid type would affect PFO pore size. As shown in Fig. 3b, the pattern of leakage was very similar to that observed in DOPC/BrPC/cholesterol vesicles, with pores formed by WT and long PFO allowing an equal extent of leakage (~30 %) of both MPTS and CB-dextrans from pelleted vesicles, while short PFO pores permit release of MPTS molecules, but not of large CB-dextran molecules. This suggests that differences in domain localization and/or lipid type do not greatly influence PFO pore size. The observation that for short PFO release of 10 and 70 kD CB-dextrans is close to zero (after subtraction of control) suggests that in the ternary mixture almost all of the pores formed by short PFO are too small to allow molecules of 10 kD or larger through.

It should be noted that although we carried out these experiments at low pH, which enhances PFO membrane insertion, and has been hypothesized to be the physiologically relevant pH, at least under some conditions (O'Brien and Melville 2004), we observed similar behavior at pH 7 (Supplemental Fig. 2).

To see if PFO pore size was somehow different for dextrans and proteins, which may not have identical shapes, we examined PFO-induced leakage of BOD-SA trapped in LUVs composed of DOPC/cholesterol and DSPC/DMoPC/cholesterol. The ~60 kD streptavidin tetramer is globular, with dimensions of ~5.5 × 4.5 × 5.0 nm (Darst et al. 1991). Figure 4 shows that in both binary and ternary lipid mixtures, the large pores formed by WT or long PFO allowed BOD-SA leakage out of the vesicles. The extent of leakage was similar to that of CB-dextrans. However, very little BOD-SA leakage was observed in the samples containing short PFO. The extent of residual leakage of BOD-SA in the presence of short PFO was very similar to that seen for large dextrans. This further confirms that the pores formed by short PFO are significantly reduced in size.

Discussion

Properties of Different Forms of PFO

We previously described the preparation and some properties of PFO molecules in which the segments that form TM β-strands were either lengthened or shortened. Several properties confirmed that the overall folding of WT, long, and short PFO in membranes is very similar (Lin and London 2013). First, all forms of PFO inserted into membranes in a strictly cholesterol-dependent fashion, in which the binding and insertion of domain 3 into membranes only occurs above a threshold cholesterol concentration. This indicates that the shortened and lengthened mutants recognize cholesterol, and thus that the cholesterol-binding domain (domain 4) is properly folded. In addition, pore formation had the same strict cholesterol dependence as membrane insertion (Lin and London 2013). This, and cholesterol-dependent membrane insertion of domain 3, would not be predicted if pore formation was just due to membrane leakiness resulting from the non-specific interaction of an improperly folded PFO aggregate with membranes.

Lengthened and shortened PFO mutants formed pore-inducing structures with specific properties that can only be explained easily in terms of their assembly into TM β-barrels. This conclusion arises from the observation that WT PFO forms pores most efficiently in bilayers with a thickness that is typical of a natural bilayer width (lipids with C18 fatty acyl chains) (Lin and London 2013). When membranes are too thick, or too thin, pore formation is less efficient (Lin and London 2013). In other words, pore formation is most efficient when there is a near-match between the length of the β-barrel and the width of the bilayer. When TM β-strands were lengthened or shortened, PFO with lengthened TM segments formed pores maximally in membranes thicker than did WT (bilayers with C20 fatty acyl chain lipids), while PFO with shortened TM segments formed pores maximally on bilayers thinner than did WT (bilayers with C16 fatty acyl chain lipids). This is exactly what would be expected if these mutations were increasing or decreasing the length of a TM β-barrel. There is also one additional line of evidence indicating that the mutated proteins in membranes formed β-barrels with TM segments that had been lengthened or shortened, rather than non-specific aggregates. When the mutants were incorporated into vesicles with co-existing lipid domains having two different thicknesses, they associated most strongly with the lipid domains having a thickness most closely matching that the length of their TM segments (Lin and London 2013) if in beta-strand form.

Alternate hypotheses for the structure of the TM, pore-forming segments in short PFO are less satisfactory. Since the segments have an alternating hydrophobic–hydrophilic they cannot form an amphiphilic helical structure with a hydrophilic face toward a pore and a hydrophobic face in contact with lipid. Furthermore, since it takes almost twice as many residues to span a bilayer for a helix relative to a β-strand, it is hard to see how any sort of TM helical

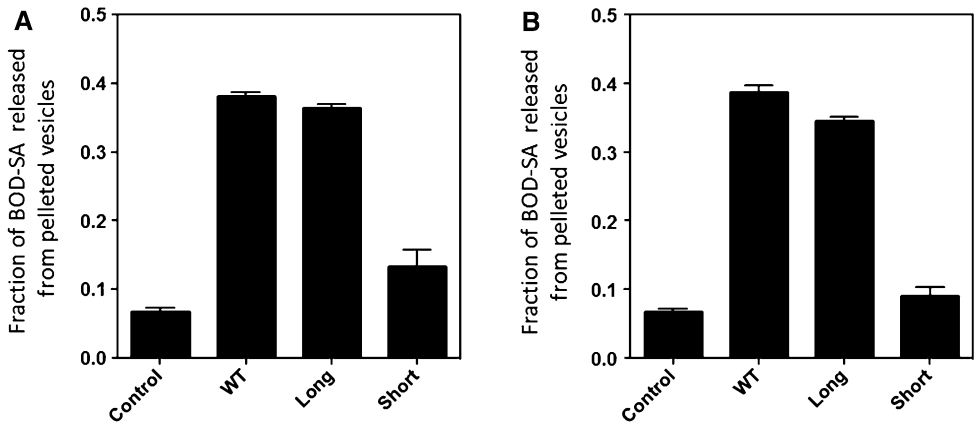

Fig. 4 Pore size of PFO mutants detected by PFO-induced BOD-SA leakage. **a** LUVs composed of 45:15:40 (mol:mol:mol) DOPC/BrPC/cholesterol with 0.002 mol% Rho-DOPE; **b** LUVs composed of 27.5:27.5:45 mol/mol/mol DSPC/DMoPC/cholesterol with 0.002 mol% Rho-DOPE. Samples containing LUVs (~500 μM lipid) entrapped BOD-SA without (Control) or with 20 μg WT, 20 μg long or 30 μg short PFO were incubated for 1 h. Final pH 5.3–5.7. After centrifugation rhodamine and BODIPY emission intensity were both measured for the resuspended pellet and supernatant. Fraction of BOD-SA in the supernatant that was released from the pelleted vesicles was calculated similar to the method in Fig. 3. Average (mean) values and SD values (*error bars*) were obtained from triplicates

hairpin structure could form. Another possibility is that in the case of short PFO the normally pore-forming segments do not form a TM structure at all, and instead pore formation reflects a simple membrane destabilization effect. However, this (or helix formation) does not fit the observed effects of membrane width upon pore formation. In particular, the observation that pores form more efficiently in intermediate width bilayers relative to thin or thick bilayers would not be expected. Instead, membrane destabilization would likely be most severe in the thinnest membranes. This model also does not explain the preference of short PFO to associate with membrane domains having a thin bilayer width.

Thus, although further studies are warranted, we conclude that it is likely that after membrane insertion mutated PFOs form TM β-barrels, with the barrel lengths expected for the mutations lengthening or shortening the TM forming sequences.

Possible Structural Implications of the Pore-Forming Properties of Mutant and WT PFO

If we assume that the model in which the changes in TM sequence length result in a shortening or lengthening of the TM β-barrel is correct, an important question is: what are the implications of pore size for how PFO structure was altered by mutation? In general, the size of the pores formed by TM β-barrel proteins is determined by the number of β-strands in the barrel and tilt angle, which is a measure of the inclination of the β-strands relative to the barrel axis (Schulz 2002). The smallest barrels contain 8 TM strands, such as the outer membrane protein A (OmpA) (Pautsch and Schulz 1998) and the outer membrane phospholipase A (OmpLA) (Snijder et al. 1999). These proteins either do not form pores, or form pores that are very small in diameter (1–2 nm), permitting flux of small molecules but not of fully folded proteins. The largest barrels of known structures are the CDCs, the class of proteins of which PFO is a member, containing up to 176 strands (Giddings et al. 2003) and creating TM pores of a remarkably large size (~30 nm in diameter).

For PFO, a tilt angle of 20° has been determined by Sato et al. (2013). Our previous studies showed that in short PFO the two-residue deletion in each TM β-strand (which shortens the strand by 6–7 Å), resulted in ~5–6 Å shortening of β-barrel TM length (Lin and London 2013), which can be explained by the deletion without a significant change in tilt angle. Furthermore, for the shortened TM strands to span a lipid bilayer one would predict that, if anything, tilt angle would decrease, which would reduce the effect of shortening the strands upon pore size. This is not what is observed. The small pores formed by short PFO were quite distinct from those formed by WT and long PFO. There appeared to be a size cutoff at close to MW 3000. A more exact size cutoff is difficult to define, because dextran molecules for any given average molecular weight actually have a range of sizes (Sharpe and London 1999), and could have different degrees of branching, which would also affect their shape and ability to pass through a pore of defined size. In addition, we cannot rule out some of heterogeneity of small pore size due to variations in oligomer size in the 4–5 range. Nevertheless, a size cutoff of 3 kD is very close to what would be predicted for the tetramer/pentamer suggested by EM. Each PFO

monomer normally contributes two membrane-inserting β-hairpins (four β-strands) to the wall of the pore (Shatursky et al. 1999). This means the pore in a tetramer or pentamer would be surrounded by 16–20 β-strands. The 19 β-strand structure of the pore-forming protein VDAC has been solved at high resolution (Bayrhuber et al. 2008; Colombini 2012). VDAC forms a pore with a diameter close to 2.5 nm, and size cutoff of 4 kD. Since a 16 β-strand barrel should have a cross-sectional area only slightly less than that of VDAC (roughly $(16/19)^2$ that of VDAC if β-strand number dominates pore size) short PFO should have either a very similar or a slightly smaller size cutoff than VDAC, which is what was observed. Of course, pore size would be affected by the size of the side chains facing the pore interior. Calculation of average side chain volume shows that pore-facing VDAC side chains are on the average very slightly larger than those of PFO so that the PFO pore might be slightly larger than predicted by the number of β-strands (not shown). In addition, formation of a short PFO pore involving a 16–20 β-strand barrel is also consistent with the 2-nm-diameter pores formed by heptametric bacterial toxins aerolysin and staphylococcal α-toxin, which are formed by a barrel with 14 β-strands (Wilmsen et al. 1992; Moniatte et al. 1996; Valeva et al. 1997).

It is interesting that the suggestion from EM that short PFO forms a tetramer or a pentamer with a pore fits the pore size data. This is unlikely to be a coincidence, and so the EM results are likely not an artifact. *Nevertheless, our conclusions do not depend on the EM data.*

Short PFO also allowed a small amount of size-independent release of larger dextran and streptavidin. One likely explanation is that short PFO forms a very small amount of large pore-forming oligomers similar to those observed for WT and long PFO. Another possibility is that short PFO induces a small amount of vesicle lysis. It should also be noted that we cannot rule out the possibility that short PFO pore size, or the ratio of small to large pores formed by short PFO, would be dependent on PFO concentration.

Although a decrease in oligomer size explains the small pore size observed with short PFO, it does not explain why shortening TM segments alters oligomer size. Presumably, the deletion of β-strand residues alters inter-strand interaction between neighboring subunits. It has been found that monomer–monomer association involves hydrogen bonding of the β1 strand from one PFO molecule to the β4 strand of the adjacent molecule (Ramachandran et al. 2004). The two residue deletion in short PFO may alter the monomer–monomer interfacial surface, so as to weaken subunit interaction and/or block PFO oligomer growth, alter inter-strand contacts, or alter β-barrel curvature in such a fashion as to result in smaller oligomers or pores.

It should also be noted that the change in structure might not be strictly due to the shortening of the TM segments, but rather due to altered interactions that result from the specific residues chosen for deletion. It is entirely possible that a different form of shortened PFO, in which different residues in the TM sequences were deleted, would form a normal oligomer and have a wild-type pore size.

Formation of a structure with a small pore by short PFO is somewhat surprising based on the conventional process by which PFO pores are assembled. It is thought that a large PFO oligomer assembles into a prepore prior to the interaction of the helical loops that form the β-barrel pore with the lipid bilayer. If the radius of the PFO ring were *irreversibly* determined at the prepore assembly step, and if the helical loops play no role in the oligomerization, the short mutant *should* have formed a large pore. However, it has not been shown that 100 % of PFO always forms the "classical" large oligomer prepore. A few percent of WT might form a small oligomer. A minor component might have been overlooked. In the short mutant, the equilibrium could favor assembly into a smaller prepore oligomer. Second, it has recently been found that the conformations formed by membrane-inserted PFO can be reversible (Lin and London 2014). A prepore might re-equilibrate after assembly between smaller and larger oligomer states, again with the large form predominating except for short PFO.

Long PFO formed the large pores characteristic of CDCs. The extent of membrane binding (Lin and London 2013), oligomer size, as estimated from EM, pore formation, and pore size were quite similar to that of WT PFO. The observation that long and WT PFO have similar pore formation and pore size suggests that the lengthened TM segments either have a greater tendency to adjust TM length by increased tilting, or the Ala insertions at the end of β-hairpin loops do not alter inter-strand interactions.

The release of entrapped molecules by WT, short, and long PFO was incomplete under the conditions we studied. This indicates that only a subpopulation of vesicles had pores. However, we estimated that there were enough PFO molecules to form 2–3 pores per vesicles, if all PFO is in the pore-forming state. Thus, either some PFO was not in the pore-forming conformation, or pores were non-randomly distributed so that some vesicles had an insufficient number of PFO molecules to form pores. The latter behavior could be present if PFO undergoes cooperative insertion into membranes, in which binding of one PFO to a vesicle helps recruit other PFO molecules.

It should be noted that shortening or lengthening PFO TM segments affects some properties of PFO in addition to pore formation. First, altering TM length alters the strength of oligomerization. Neither long nor short PFO forms the SDS-resistant oligomers observed with WT PFO (Shepard

et al. 2000). Second, as shown previously, the mutated segments have somewhat different local conformations in aqueous solution. The sequences forming the TM β-hairpins after membrane insertion are packed as two sets of three α-helices when in aqueous solution prior to membrane insertion (Shepard et al. 1998; Shatursky et al. 1999). Acrylodan labeling studies show that the environment of residue 215 in these hairpins is more hydrophobic for long and short PFO with (acrylodan emission $\lambda_{max} = 483$ nm), than for WT PFO ($\lambda_{max} = 504$ nm) (Lin and London 2013). Finally, proper folding of short PFO was less (66 %) than that of WT and long PFO based on the fraction of molecules that bind to lipid (Lin and London 2013).

Biological and Biomedical Applications of Pore-Forming Proteins with Different Pore and TM Lengths

Relative to multi-TM α-helix proteins, β-barrel structures are especially amenable to engineering of TM segment properties to adjust their properties for various applications. Prior studies have demonstrated that various modifications in the coding genes can be introduced without affecting β-barrel structure in membranes (Koebnik 1999). This, added to the range of pore sizes that can be formed by such proteins (see above), makes them attractive targets for engineering pores with various sizes.

Many mutations in pore-forming β-barrel proteins have the goal of altering pore properties. Widely used approaches for pore-forming protein engineering mainly involve straight genetic engineering or targeted chemical modification (Bayley and Jayasinghe 2004). Several mutations in the pore eyelet of the porin from *Rhodopseudomonas blastica* have been reported (Schmid et al. 1998), altering size and charge selectivity of the pore. In another study, a substitution introducing either 7 or 14 Arg near the narrowest part of the pore formed by the heptameric α-hemolysin protein acted as primitive binding site for channel blockers (Cheley et al. 2002). Other studies have shown that modification of residues on the interior of the α-hemolysin cap with a covalently bound poly(ethylene glycol) (PEG) chain (Movileanu et al. 2000) or introducing a non-covalent adaptor β-cyclodextrin within its lumen modulates the size and selectivity of α-hemolysin pores (Yannakopoulou et al. 2011). Our results provide an additional new approach for engineering the properties of pore-forming proteins. By altering the TM β-strand lengths, we have shown that the architectural arrangement of β-strands can be changed in a fashion that alters β-barrel and pore size. It is even possible that hybrid oligomers with a wider range of sizes could be generated by mixing mutant PFO and WT PFO with different ratios.

Pore-forming proteins can be used for permeabilization of cells (Walev et al. 2001), and engineering pore size could lead to useful applications in medicine to attack malignant cells or for drug delivery. There may be additional applications for β-barrel proteins with engineered TM lengths. As noted above, we recently demonstrated that due to hydrophobic mismatch between TM barrel length and membrane domains width, the length of TM segments affects multi-TM segment protein partitioning into lipid rafts (Lin and London 2013). This indicates that engineered PFO pores could be useful for local targeting. For example, through coupling to engineered PFO, drugs or other macromolecules could be introduced so as to interact with specific proteins located within or outside of raft domains in cell membranes.

Acknowledgments The authors thank Prof. A. Heuck, (U. Mass. Amherst) for providing protocols to prepare BODIPY-labeled streptavidin. This work was supported by NSF Grant MCB 1019986.

References

Aroian R, Van Der Goot FG (2007) Pore-forming toxins and cellular non-immune defenses (CNIDs). Curr Opin Microbiol 10:57–61

Bayley H, Jayasinghe L (2004) Functional engineered channels and pores (Review). Mol Membr Biol 21:209–220

Bayrhuber M, Meins T, Habeck M, Becker S, Giller K, Villinger S, Vonrhein C, Griesinger C, Zweckstetter M, Zeth K (2008) Structure of the human voltage-dependent anion channel. Proc Natl Acad Sci USA 105:15370–15375

Bhakdi S, Tranum-Jensen J (1984) Mechanism of complement cytolysis and the concept of channel-forming proteins. Philos Trans R Soc Lond B Biol Sci 306:311–324

Cassidy SK, O'riordan MX (2013) More than a pore: the cellular response to cholesterol-dependent cytolysins. Toxins (Basel) 5:618–636

Cheley S, Gu LQ, Bayley H (2002) Stochastic sensing of nanomolar inositol 1,4,5-trisphosphate with an engineered pore. Chem Biol 9:829–838

Cheng HT, London E (2011) Preparation and properties of asymmetric large unilamellar vesicles: interleaflet coupling in asymmetric vesicles is dependent on temperature but not curvature. Biophys J 100:2671–2678

Chiu J, March PE, Lee R, Tillett D (2004) Site-directed, ligase-independent mutagenesis (SLIM): a single-tube methodology approaching 100 % efficiency in 4 h. Nucleic Acids Res 32:e174

Chiu J, Tillett D, Dawes IW, March PE (2008) Site-directed, ligase-independent mutagenesis (SLIM) for highly efficient mutagenesis of plasmids greater than 8 kb. J Microbiol Methods 73:195–198

Colombini M (2012) VDAC structure, selectivity, and dynamics. Biochim Biophys Acta 1818:1457–1465

Darst SA, Ahlers M, Meller PH, Kubalek EW, Blankenburg R, Ribi HO, Ringsdorf H, Kornberg RD (1991) Two-dimensional crystals of streptavidin on biotinylated lipid layers and their interactions with biotinylated macromolecules. Biophys J 59:387–396

Fussle R, Bhakdi S, Sziegoleit A, Tranum-Jensen J, Kranz T, Wellensiek HJ (1981) On the mechanism of membrane damage by *Staphylococcus aureus* alpha-toxin. J Cell Biol 91:83–94

Giddings KS, Johnson AE, Tweten RK (2003) Redefining cholesterol's role in the mechanism of the cholesterol-dependent cytolysins. Proc Natl Acad Sci USA 100:11315–11320

Hotze EM, Tweten RK (2012) Membrane assembly of the cholesterol-dependent cytolysin pore complex. Biochim Biophys Acta 1818:1028–1038

Koebnik R (1999) Structural and functional roles of the surface-exposed loops of the beta-barrel membrane protein OmpA from *Escherichia coli*. J Bacteriol 181:3688–3694

Lin Q, London E (2013) Altering hydrophobic sequence lengths shows that hydrophobic mismatch controls affinity for ordered lipid domains (rafts) in the multitransmembrane strand protein perfringolysin O. J Biol Chem 288:1340–1352

Lin Q, London E (2014) The influence of natural lipid asymmetry upon the conformation of a membrane-inserted protein (perfringolysin O). J Biol Chem 289:5467–5478

Ludtke SJ, Baldwin PR, Chiu W (1999) EMAN: semiautomated software for high-resolution single-particle reconstructions. J Struct Biol 128:82–97

Mitsui K, Sekiya T, Okamura S, Nozawa Y, Hase J (1979) Ring formation of perfringolysin O as revealed by negative stain electron microscopy. Biochim Biophys Acta 558:307–313

Moniatte M, Van Der Goot FG, Buckley JT, Pattus F, Van Dorsselaer A (1996) Characterisation of the heptameric pore-forming complex of the Aeromonas toxin aerolysin using MALDI-TOF mass spectrometry. FEBS Lett 384:269–272

Movileanu L, Howorka S, Braha O, Bayley H (2000) Detecting protein analytes that modulate transmembrane movement of a polymer chain within a single protein pore. Nat Biotechnol 18:1091–1095

Nelson LD, Johnson AE, London E (2008) How interaction of perfringolysin O with membranes is controlled by sterol structure, lipid structure, and physiological low pH—insights into the origin of perfringolysin O-lipid raft interaction. J Biol Chem 283:4632–4642

Nelson LD, Chiantia S, London E (2010) Perfringolysin O association with ordered lipid domains: implications for transmembrane protein raft affinity. Biophys J 99:3255–3263

O'Brien DK, Melville SB (2004) Effects of *Clostridium perfringens* alpha-toxin (PLC) and perfringolysin O (PFO) on cytotoxicity to macrophages, on escape from the phagosomes of macrophages, and on persistence of *C. perfringens* in host tissues. Infect Immun 72:5204–5215

Parker MW, Feil SC (2005) Pore-forming protein toxins: from structure to function. Prog Biophys Mol Biol 88:91–142

Pautsch A, Schulz GE (1998) Structure of the outer membrane protein A transmembrane domain. Nat Struct Biol 5:1013–1017

Ramachandran R, Tweten RK, Johnson AE (2004) Membrane-dependent conformational changes initiate cholesterol-dependent cytolysin oligomerization and intersubunit beta-strand alignment. Nat Struct Mol Biol 11:697–705

Rosconi MP, Zhao G, London E (2004) Analyzing topography of membrane-inserted diphtheria toxin T domain using BODIPY-streptavidin: at low pH, helices 8 and 9 form a transmembrane hairpin but helices 5–7 form stable nonclassical inserted segments on the cis side of the bilayer. Biochemistry 43:9127–9139

Rossjohn J, Feil SC, Mckinstry WJ, Tweten RK, Parker MW (1997) Structure of a cholesterol-binding, thiol-activated cytolysin and a model of its membrane form. Cell 89:685–692

Sato TK, Tweten RK, Johnson AE (2013) Disulfide-bond scanning reveals assembly state and beta-strand tilt angle of the PFO beta-barrel. Nat Chem Biol 9:383–389

Scherrer R, Gerhardt P (1971) Molecular sieving by the *Bacillus megaterium* cell wall and protoplast. J Bacteriol 107:718–735

Schmid B, Maveyraud L, Kromer M, Schulz GE (1998) Porin mutants with new channel properties. Protein Sci 7:1603–1611

Schulz GE (2002) The structure of bacterial outer membrane proteins. Biochim Biophys Acta 1565:308–317

Sharpe JC, London E (1999) Diphtheria toxin forms pores of different sizes depending on its concentration in membranes: probable relationship to oligomerization. J Membr Biol 171:209–221

Shatursky O, Heuck AP, Shepard LA, Rossjohn J, Parker MW, Johnson AE, Tweten RK (1999) The mechanism of membrane insertion for a cholesterol-dependent cytolysin: a novel paradigm for pore-forming toxins. Cell 99:293–299

Shepard LA, Heuck AP, Hamman BD, Rossjohn J, Parker MW, Ryan KR, Johnson AE, Tweten RK (1998) Identification of a membrane-spanning domain of the thiol-activated pore-forming toxin *Clostridium perfringens* perfringolysin O: an alpha-helical to beta-sheet transition identified by fluorescence spectroscopy. Biochemistry 37:14563–14574

Shepard LA, Shatursky O, Johnson AE, Tweten RK (2000) The mechanism of pore assembly for a cholesterol-dependent cytolysin: formation of a large prepore complex precedes the insertion of the transmembrane beta-hairpins. Biochemistry 39:10284–10293

Snijder HJ, Ubarretxena-Belandia I, Blaauw M, Kalk KH, Verheij HM, Egmond MR, Dekker N, Dijkstra BW (1999) Structural evidence for dimerization-regulated activation of an integral membrane phospholipase. Nature 401:717–721

Tang G, Peng L, Baldwin PR, Mann DS, Jiang W, Rees I, Ludtke SJ (2007) EMAN2: an extensible image processing suite for electron microscopy. J Struct Biol 157:38–46

Tweten RK (2005) Cholesterol-dependent cytolysins, a family of versatile pore-forming toxins. Infect Immun 73:6199–6209

Valeva A, Palmer M, Bhakdi S (1997) Staphylococcal alpha-toxin: formation of the heptameric pore is partially cooperative and proceeds through multiple intermediate stages. Biochemistry 36:13298–13304

Walev I, Bhakdi SC, Hofmann F, Djonder N, Valeva A, Aktories K, Bhakdi S (2001) Delivery of proteins into living cells by reversible membrane permeabilization with streptolysin-O. Proc Natl Acad Sci USA 98:3185–3190

Wang J, London E (2009) The membrane topography of the diphtheria toxin T domain linked to the a chain reveals a transient transmembrane hairpin and potential translocation mechanisms. Biochemistry 48:10446–10456

Wilmsen HU, Leonard KR, Tichelaar W, Buckley JT, Pattus F (1992) The aerolysin membrane channel is formed by heptamerization of the monomer. EMBO J 11:2457–2463

Yannakopoulou K, Jicsinszky L, Aggelidou C, Mourtzis N, Robinson TM, Yohannes A, Nestorovich EM, Bezrukov SM, Karginov VA (2011) Symmetry requirements for effective blocking of pore-forming toxins: comparative study with alpha-, beta-, and gamma-cyclodextrin derivatives. Antimicrob Agents Chemother 55:3594–3597